JOURNAL OF PHYSICAL ORGANIC CHEMISTRY, VOL. 10, 737–746 (1997)

SPECTRAL AND KINETIC MEASUREMENTS ON A SERIES OF PERSISTENT IMINOXYL RADICALS

BRIAN M. EISENHAUER,† MINGHUI WANG,‡ RICHARD E. BROWN, HENRYK LABAZIEWICZ,§ MARIA NGO,¶ KARL W. KETTINGER‖ and G. DAVID MENDENHALL*

Department of Chemistry, Michigan Technological University, Houghton, Michigan 49931-1295, USA

A series of new iminoxyl radicals, $Et_3C(C=NO^{\bullet})Bu$-*tert* (1), *tert*-$C_5H_{11}(C=NO^{\bullet})$ Bu-*tert* (2), (*tert*-$C_5H_{11})_2C=NO^{\bullet}$ (3), $Et_3C(C=NO^{\bullet})Ph$ (4), $PhCH_2CMe_2(C=NO^{\bullet})Bu$-*tert* (5), $PhCMe_2(C=NO^{\bullet})Bu$-*tert* (6) and $Me_2CH(C=NO^{\bullet})C_5H_{11}$-*tert* (7), was characterized by EPR and in some cases visible spectra and decay kinetics in solution. Isolation of 1H and 3-*tert*-butyl-4,4-diethyl-5-methyl-4,5-dihydro-5-isoxazolol (9) among the decomposition products of 1 was consistent with a previously unrecognized mode of iminoxyl reaction in which the initial step is an internal β-H abstraction. Molecular orbital calculations on $H_2C=NO^{\bullet}$ indicate a C–N–O angle of about 140° and a 10 kcal mol^{-1} barrier to inversion. Rate constants for the reaction of *tert*-$Bu_2C=NO^{\bullet}$ (8) with a series of olefins were measured. © 1997 John Wiley & Sons, Ltd.

J. Phys. Org. Chem. **10**, 737–746 (1997) No. of Figures: 6 No. of Tables: 5 No. of References: 26

Keywords: iminoxyl radicals; spectra; kinetics

Received 12 February 1997; revised 17 April 1997; accepted 17 April 1997

INTRODUCTION

Iminoxyl radicals (general formula $R_2C=NO^{\bullet}$) are a large class of reactive radicals that have been characterized at low concentrations by ESR spectra[1] and kinetics.[2] The radicals are easily generated by oxidation of the corresponding oximes, possibly including ones of biological importance involved in nitric oxide metabolism.[3] Most iminoxyls decay by primary pathways of reversible and irreversible dimerization (Scheme 1).

The products isolated from the oxidation of oximes are varied and usually include species arising from secondary reactions of the decomposition products.[2,4] The conversion of oximes to ketones with oxides of nitrogen, during which iminoxyls are likely intermediates, is regarded as a standard synthetic transformation.[5] Head-to-tail dimerization as shown below is the exclusive pathway in the initial stages for di-*tert*-butyl ketiminoxyl (**8**),[4] and probably also for bis(1-adamantyl) ketiminoxyl.[6]

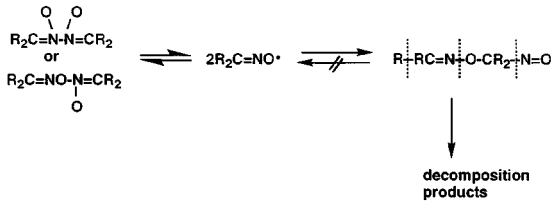

Scheme 1

EXPERIMENTAL

The syntheses of the oximes and radicals are described elsewhere.[7] Reagent chemicals were purchased from commercial sources. Olefins and oxidizable solvents were passed through a short column of alumina before use.

The kinetics of decay of iminoxyl radicals by ESR were measured from relative peak heights in the first-derivative spectrum (< 1 mM) or the doubly-integrated areas (> 1 mM) from scans on a Varian E9 spectrometer. Initial concentrations of radicals were determined by radical weight (for isolable radicals) or by comparison with the ESR spectra of

* *Correspondence to:* G. D. Mendenhall. E-mail gdmenden@mtu.edu

† Present address: Peninsula Copper Industries, Inc., 1700 Duncan Ave, Hubbell, MI 49934, USA.

‡ Present address: Department of Chemistry, State University of New York at Stony Brook, Stony Brook, NY 11794, USA.

§ Present address: Department of Chemistry, University of Miami, P.O. Box 249118, Coral Gables, FL 33124, USA.

¶ Present address: Environmental Analytical Research Laboratory, Dow Chemical Co., Midland, MI 48641, USA.

‖ Present address: Janssen Research Foundation, 655 Pheonix Drive, Ann Arbor, MI 48108, USA.

Contract grant sponsor: US Army Research Office; *Contract grant number:* DAAG 29-78-C-001.

Contract grant sponsor: Petroleum Research Fund.

CCC 0894–3230/97/100737–10 $17.50

standard solutions of persistent radicals (**8** or 2′,2′-diphenylpicrylhydrazyl). The rates of decay were followed by the loss of absorbance at 800 nm either (a) in a 1-cm quartz cell in an HP Model 8451A diode-array spectrometer operated in a programmed mode to print out absorbances at regular intervals, or (b) for longer-term experiments, in a 0·5 cm cell attached at an angle to the middle of a 10 mm tube sealed at one end (Figure 1). The sample was placed in the sealed end of the tube, which was then attached to a vacuum line for degassing, and sealed off with a torch. After thawing, the container was stored in a constant-temperature water bath and removed for periodic optical measurements. A cut-off filter eliminating wavelengths below 600 nm was interposed in the light path of the diode array to prevent photolytic regeneration of the radical during the measurements. The decay of **1** was also monitored in separate experiments by HPLC (150 × 4 mm i.d. C_{18} column, acetonitrile–water (90:10) eluent, refractive index detection with a Knauer Model 37 instrument).

Decomposition of *tert*-butyl 1,1-diethylpropyl ketiminoxyl (1) in di-*tert*-butyl nitroxide. A mixture of freshly prepared **1** (15·3 mg, 76·9 μmol) and di-*tert*-butyl nitroxide [24·7 mg, 171 μmol (Aldrich), both radicals purified by elution through basic alumina with pentane before use) were mixed in a small vial with an aluminum–silicone crimp seal. The initial concentration of **1** was about 1·7 M. Aliquots of 1.0 μl were withdrawn periodically, diluted with 10 ml of hexanes in a volumetric flask and the diluted samples were stored at −60 °C until all were analyzed by ESR (25 °C) at one time under identical conditions. The average peak-to-peak heights of the two outer lines of each radical, which were well resolved from signals from the other radical, were recorded for each sample.

Reaction of di-*tert*-butyl ketiminoxyl (8) with cyclohexene. Reactions of **8** with cyclohexene and with some other olefins in argon-flushed solutions in isooctane at 28 ± 1 °C were followed by the decrease in absorbance at 800 nm in a 1 cm quartz cell in the diode-array spectrometer as described above. A control experiment with 0·103 M radical in isooctane alone showed a decrease of about 0·002 M after 4 h (maximum time for experiments with olefins, 4·5 h) under these conditions.

THEORETICAL

Molecular orbital method

Ab initio calculations were carried out on both formaldoxime, H_2CNOH, and its iminoxyl radical, H_2CNO. The primary motivation was to determine the geometry of the radical and clarify the preferred isomerization pathway rather than to obtain a comprehensive mapping of the potential energy surfaces. The molecular orbital calculations were carried out using the Gaussian 90 and Gaussian 92 suites of programs.[8] Several levels of theory were used to establish the reliability of the final results used in this study. Geometries were optimized at the unrestricted Hartree–Fock (UHF) and unrestricted second-order Møller–Plesset perturbation (UMP2) theory levels with analytical gradient techniques.[9] A variety of basis sets were used, which included different single and split valence sets with and without diffuse and polarization functions.[10] These included the STO-3G, 3–21G, 6–31G/d) and the 6–31++G(2df,p) sets. In all cases, all geometical parameters were fully optimized using the frozen core approximation.

For both molecules, the energy was also optimized at the UMP4/6–31g(d) level using a numerical procedure. The harmonic UHF/6–31G(d) vibrational frequencies were determined to verify the authenticity of the stationary points as minima or transition states and to determine the zero point energies (ZPE). These were scaled by a factor of 0·98 to correct for the well documented overestimation of the vibrational frequencies at the Hartree–Fock level.

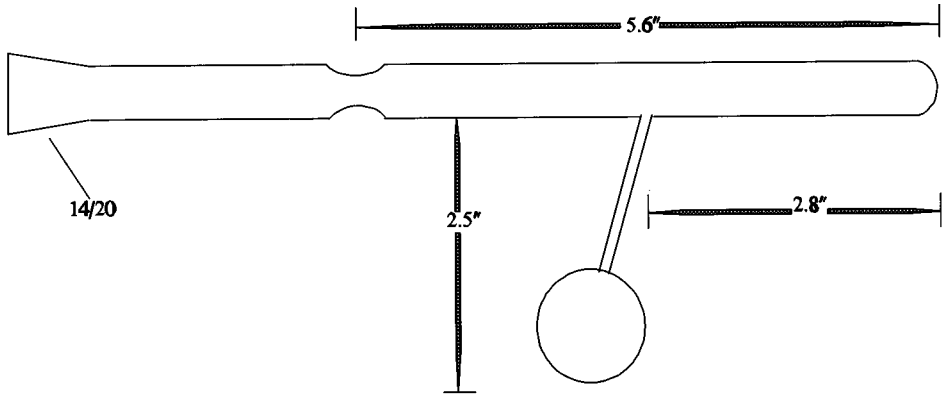

Figure 1. Apparatus for preparation of solutions of iminoxyl radical for measurement of decay kinetics in optical cell

Spin contamination

For representing doublet states with UHF functions, there is some concern regarding the spin contamination from the higher spin states, particularly the quartet. Often when the expectation value of the spin angular momentum operator, $\langle S^2 \rangle$, is much larger than the exact value of 0·75 for the doublet, some measure of the effect of the contamination on the molecular properties such as the geometry, energy and inversion barriers should be made. This was accomplished here by comparing the UHF geometries to the ROHF (restricted open-shell Hartree–Fock) geometries and the ROHF, PUHF (spin projected UHF) and PUMP2 (spin projected UMP2) energy profiles to the UHF and UMP2 values. The PUMP2 values are those calculated after projecting out the quartet contaminant. If the geometries and energy profiles are similar for the test cases, the contamination will be considered to be not significant. Most of the test cases were made on only the H_2CNO, CH_3CHNO and CH_2CHNOH molecules, since these are representative of the larger systems. The slowly convergent ROHF method made it too time consuming to apply to the larger systems studied here.

RESULTS AND DISCUSSION

Iminoxyl decomposition pathways

Radical **1** was the first of the new radicals to be isolated in this study. It could be preserved for long periods at -50 °C; the stability increased with dilution, but kinetic data from a series of starting concentrations did not correspond to a simple second-order process (Figure 2).

Further investigation of the decomposition products of **1** revealed 9–11 products (HPLC), traces of pivalonitrile and triethylacetonitrile, but no detectable 4,4-diethyl-2,2-dimethylhexan-3-one (<1%). In striking contrast, radical **8** on standing gave about 4% pivalonitrile and 40% di-*tert*-butyl ketone.[4]

A possible decay sequence for the radical, constistent with the limited evidence, is given in Scheme 2.

Iminoxyls are known to exchange H-atoms with oximes slowly,[11] which can account for the appearance of the parent oxime among the decomposition products of **1**. In addition, the regeneration of iminoxyls from iminyls ($R_2C{=}N^{\bullet}$) and oxygen, and the β-scission of iminyls into nitriles are both known reactions.[12] The isolation of **9** and **1H** from the decomposition of **1** are described elsewhere.[7]

The inference that the weaker but sterically more hindered methylene hydrogens were abstracted is suggested by an experiment in which di-*tert*-butyl nitroxide was a solvent for **1**, which decomposed without significantly changing the concentration of the nitroxide (Figure 3). Spin-trapping rate constants by di-*tert*-butyl nitroxide have been shown to be sensitive to steric effects.[13]

The other radicals were not examined in detail. Radicals **2** and **3** decayed slightly faster than the more heavily substituted radical **1**. The kinetics of iminoxyls that were highly unstable could be monitored quickly to a high degree of consumption, and the distinction between a first- and second-order decay in those cases was especially clear. Most disappeared by second-order kinetics (Table 1) at the concentrations examined.

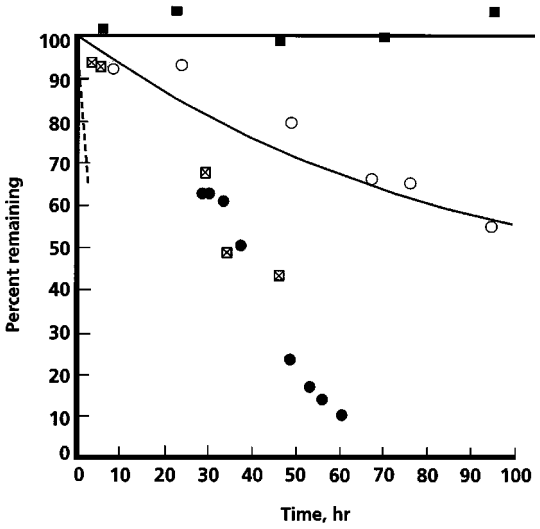

Figure 2. Plots of residual $Me_3C(C{=}NO^{\bullet})CEt_3$ (**1**) in benzene at ambient temperature with time as a function of initial concentrations, which were (■ $9{\cdot}4\times10^{-5}$ M, by ESR; (○) 0·019 M, 800 nm; (⊠ 1·6 M, ESR; and (●) 4·7 M, neat, ESR. The dashed line is the decay curve predicted for an initial concentration of 1·6 M and a second-order decay constant derived from the decay curve with an initial concentraton of 0·019 M

Spectral data

The three new iminoxyls that could be isolated were blue liquids which displayed the characteristic intense band at 1605 (radical **1**) or 1607 cm^{-1} (others). All of the iminoxyls at high dilution showed a 1:1:1 triplet due to the characteristic ^{14}N ($I=1$) hyperfine splitting with $a_N \approx 30$ G, and similar g values near 2·005 (Table 2).

Each of the triplets in the EPR spectra displayed proton hyperfine coupling, which was recorded at a series of temperatures in a search for optimal resolution. The best spectra were simulated with a computer program[14] which, with carefully selected parameters, gave satisfactory fits to the experiental spectra in all but two cases. The photochemically genrated ESR spectrum, ascribed to **4**, from 2′,2′-diethylbutyrophenone oxime and di-*tert*-butyl peroxide showed a triplet whose fine structure differed from one another, indicating an overlap of two radicals, probably the *syn* and *anti* iminoxyls. The three spectral multiplets in the ESR spectrum of *tert*-amyl *iso*propyl ketiminoxyl (**7**) wee also asymmetric, and only the average nitrogen splitting could be determined.

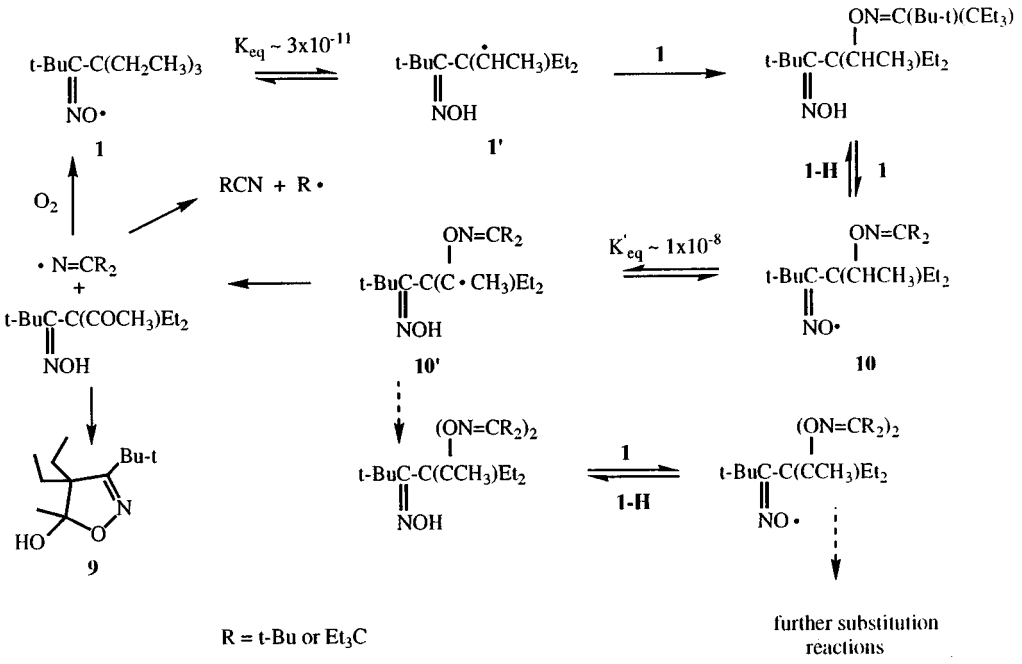

Scheme 2

The simulated values of a_N and a_H are unexceptional. Except for two radicals giving complicated spectra, and one other exception, the simulations were sufficient with appropriate values for a_N, and individual values of a_H with multiplicities corresponding to the numbers of equivalent α, β and γ hydrogens only. The third exception was 1,1-dimethylphenethyl *tert*-butyl ketiminoxyl (**5**), whose ESR spectrum could not be simulated until three hydrogens were deleted from the input. One possible inference from this result is that the *tert*-butyl rotation is slow on the conventional ESR time-scale.

Cumyl *tert*-butyl ketiminoxyl (**6**) showed a visible absorption spectrum similar to that of other isolable iminoxyls with an absorption envelope peaking near 800 nm. This spectrum could be generated by UV irradiation of solutions of the oxime in solvents containing di-*tert*-butyl peroxide, and the decay of the signal with time was analyzed under the assumption that the iminoxyl absorption coefficient was the same as the di-*tert*-butyl analogue (**8**).

The decay of the 800 nm band of **8**, an isolable iminoxyl, was also followed in mixtures of radical and cyclohexene or other olefin. Second-order rate constants derived from the data are shown in Table 3

Molecular orbital calculations

The energy and geometries are given in Tables 4 and 5 for H_2CNO and H_2CNOH, respectively, for a variety of methods along with some of the pertinent experimental data which is available. Both molecules were essentially planar at their global minimum. The expectation values of the spin operator, $\langle S^2 \rangle$, show some worrisome deviations from the exact value of 0·75 for a doublet state. To test the effect of the spin contamination on the properties of H_2CNO, ROHF calculations were completed and the PUHF and PUMP2 energies were determined from the spin projected UHF and UMP2 results. None of these results change any of the conclusions reached and the unrestricted or unprojected calculations. More specifics are given in the discussion below. For H_2CNO, the $^2A'$ state was always lower than the $^2A''$ state except at small CNO bond angles approaching 90° where the two states became nearly degenerate. In both H_2CNO and H_2CNOH, the hydrogen atom labeled H_1 is *syn* to the oxygen atom while the other, H_2, is the *anti* configuration. In H_2CNOH, the hydroxyl hydrogen is in the *anti* configuration to the carbon atom. For the iminoxyl radical, H_2CNO, a high-level of theory with a good basis set was necessary before the geometry converged to consistent values. These gave values close to 140° for the CNO angle which agree very well with values which Fox and Symons[15] calculated from the ESR spectra of 13 substituted iminoxyl radicals [137° < Θ(CNO) < 143°]. The importance of including correlation is shown by the results with the UHF/6–31G(d) method, which gives a CNO bond angle of only 125°, close to calculated values in the literature based on the INDO method.[16]

We used the MP2/6–31(G) method to calculate the

energy profiles as illustrated in Figure 4. The energy profiles are for the extension of the CNO angle where all other parameters were optimized at each point. The energies are in kcal mol^{-1} (1 kcal = 4·184 kJ) and are relative to the global minimum energy of each molecule as given in Tables 4 and 5. This method has been demonstrated to give reliable geometries, and in this work gives a good reproduction of the H_2CNOH experimental geometries as determined from Levine's microwave study and listed as Table 5.[17,18] Comparisons can be also made with the x-ray crystallographic results on dimethylglyoxime and *p*-chlorobenzaldoxime.[19,20] Additionally, for H_2CNO using the UMP2 method, the 6–31g(d) basis reproduces the geometry using the more extensive 6–31++G(2df,p) basis; all of the geometrical parameters from the two sets are within 1% of each other. As a check on the effect of the residual electronic correlation, Figure 4 also has the profile for H_2CNO calculated with the UMP4/6–31G(d)//UMP2/6–31G(d) method. The UMP2 and UMP4 curves are almost graphically indistinguishable. The UMP4/6–31G(d) optimized

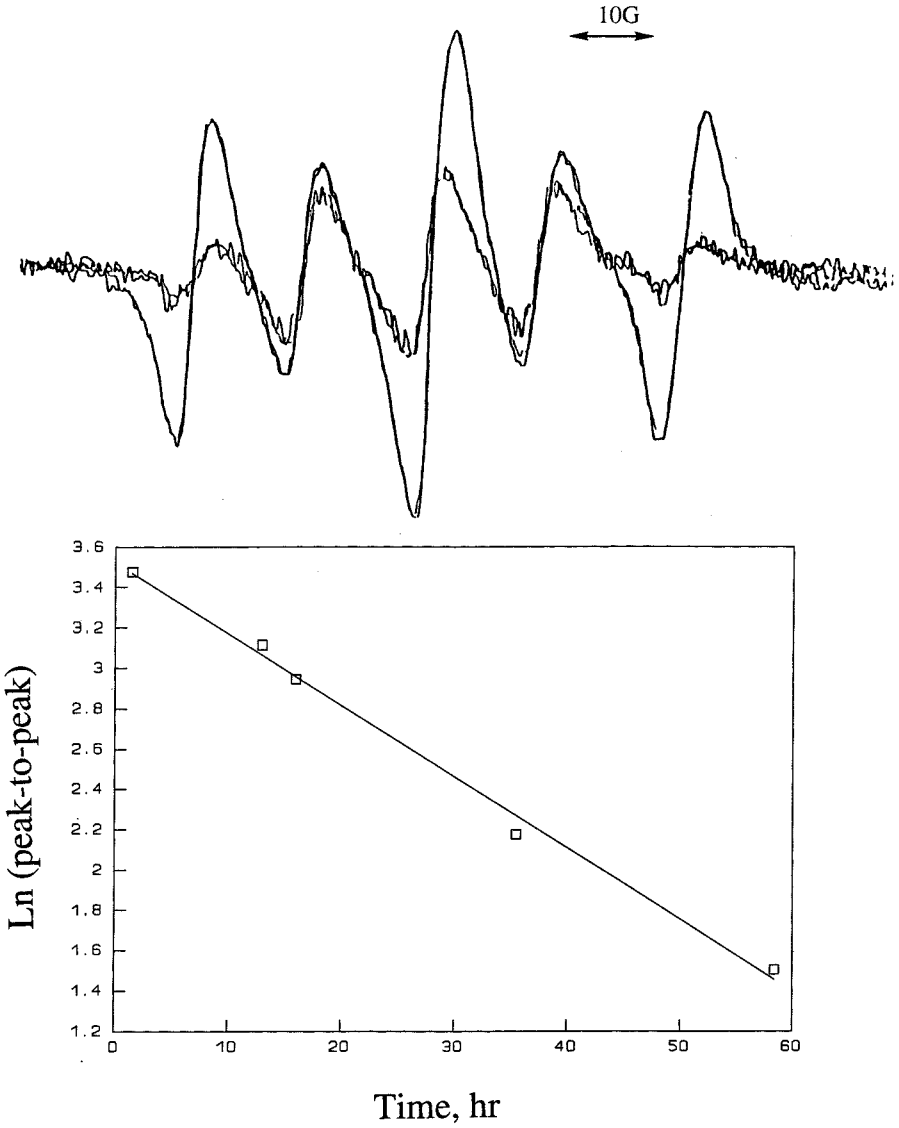

Figure 3. (Top) ESR spectrum from a qualitative study of a reaction mixture of radical **1** and di*tert*-butyl nitroxide in hexanes, initially and after several days, and (bottom) semilogarithmic plot of relative concentration of **1** (initially 1·7 M) vs time in a neat mixture of the two radicals (see Experimental for details)

Table 1. Rate constants for decay of iminoxyl radicals (24±2 °C)

Iminoxyl	C_0 (M)	Solvent	Method	Rate constant
8	0·2	C_6H_6	800 nm	$[2k_2 = 2.1 \times 10^{-5}$ M^{-1} s$^{-1}]$[a]
2	0·1			$2k_2 = 6.3 \times 10^{-5}$ M^{-1} s^{-1}
3	0·1			$2k_2 = 6.9 \times 10^{-5}$ M^{-1} s^{-1}
1	0·1			$2k_2 = 1.4 \times 10^{-5}$ M^{-1} s^{-1}[a]
7	0·012[b]	2:1 v/v BOOB[c]–C_6H_6	ESR	$2k_2 = 0{\cdot}17$ M^{-1} s^{-1}[d]
			800 nm	$2k_2 = 0{\cdot}05$ M^{-1} s^{-1}[d,e]
5	0·0030[b]	2:1 v/v BOOB–C_6H_6	ESR	$2k_2 = 0{\cdot}56 \pm 0{\cdot}09$ M^{-1} s^{-1}[f]
4	~0·001[b]	1:4 v/v BOOB–C_6H_6	ESR	$k_1 = (3{\cdot}4–15) \times 10^{-4}$ s^{-1}[g]
			800 nm	$k_1 = (7{\cdot}2–16) \times 10^{-4}$ s^{-1}[e,g]
		BOOB	ESR	$k_1 = 1{\cdot}5 \times 10^{-3}$ s^{-1}
			800 nm	$k_1 = 1{\cdot}6 \times 10^{-3}$ s^{-1}[e]
6	0·0024[b,h]	1:7 v/v BOOB–C_6H_6	800 nm	$2k_2 = 0{\cdot}66$ M^{-1} s^{-1}[e]
	0·00088		ESR	$2k_2 = 0{\cdot}65$ M^{-1} s^{-1}
	0·000060			$2k_2 = 0{\cdot}68$ M^{-1} s^{-1}
X(tBuC=NO•)$C_{10}H_{14}$[i]	0·0048	2:1 THF–C_6H_6	800 nm	$2k_2 = 0{\cdot}041$ M^{-1} s^{-1}[e]

[a] Ref. 4.
[b] Generated photochemically from solution of oxime in solvent.
[c] Di-*tert*-butyl peroxide.
[d] Initial decay only, assumed second order.
[e] Assuming $\varepsilon = 5.1$ as found for di-*tert*-butyl analog.
[f] Average of three decays.
[g] First-order rate constants refer to observed ranges of the decay of the ESR signal.
[h] Decay after first photolysis of solution (after subsequent photolyses decay was faster and first order).
[i] Iminoxyl radical from Ag_2O and 1,3-dipivaloyladamantane bisoxime, at 28 °C.

geometries reported in Tables 4 and 5 also agree very well with their UMP2 counterparts. The only significant exception was a difference of 3° in the value of the CNO angle in the H_2CNO molecule, which exhibited a broad shallow minimum for this angle. Most of a considerable body of previous theoretical work has focused on formaldoxime and its protonated or deprotonated ions and less on the comparison between formaldoxime and its iminoxyl radical.[21]

To illustrate the effects of spin contamination in H_2CNO, also in Figure 4 are plotted the energy profiles for the UHF/6–31g(d) and ROHF/6–g)d) methods where all parameters were again optimized for each CNO angle. These two methods give very similar results. Profiles using the PUHF and PUMP2 methods could hardly be graphically differentiated from those of the UHF and UMP2 methods and are not presented here. This and the results in Table 4 indicate that the spin contamination has little effect on these conclusions. In fact, the effects from the inclusion of electronic correlation at the MP2 or MP4 levels are much

Table 2. ESR coupling constants for iminoxyl radicals

Iminoxyl	Solvent	T (°C) for a_H	g[a]	a_N (G)[a]	a_H (G)
8	C_6H_6	Ambient	2·00522[b]	31·32[b]	0·481 (9H), 0·772 (9H)[c]
2		21	2·0054	31·3	0·76 (9H), 0·67 (6H), 0·48 (2H)
3		−40	2·0052	31·3	0·69 (6H), 0·60 (6H), 1·11 (2H), 1·17 (2H)
1	Alkane[d]	130	2·0051[e]	31·3	0·52 (9H), 0·49 (6H)
7	2:1 BOOB–C_6H_6	−40	2·0050	31·3	1·42 (6H), 0·30 (2H), 4·17 (1H)
5		−40	2·0050	31·3	0·99 (6H), 0·53 (3H), 0·36 (3H), 0·60 (2H)
4		Ambient	2·0053	31·6, 31·7[f]	—
6		40	2·0053	31·0	0·82 (9H), 0·71 (6H)
X(tBuC=NO•)$C_{10}H_{14}$[g]	C_6H_6	Ambient	2·0053	31·6	—[h]

[a] All g and a_N values determined at ambient temperature.
[b] Data from Ref. 4.
[c] Data from Ref. 22.
[d] a_N at 21 °C in pentane, a_H at 130 °C in decane.
[e] In benzene.
[f] Two overlapping radicals present.
[g] Structure uncertain (see text).
[h] Proton splitting apparent but not completely resolved.

Table 3. Rate constants for reaction of **8** with hydrocarbons (isooctane, 28 ± 1 °C)

$[Radical]_0$ (M)	$[RH]_0$ (M)	$10^5\ k_{obs}$ (s^{-1})[a]	$10^5\ k_{obs}/2\ [RH]_0$ $(M^{-1}\ s^{-1})$
0·16	0·85 cyclohexene	6·17	3.6
0·094	9·86	87·15	4·4
			Mean: 4·0 ± 0·5
0·29	0·77 cyclopentadiene	6·89	4·5
0·05	5·7	64·4	5·7
0·07	4·7	46·7	5·0
			Mean: 5·1 ± 0·5
0·07	3·0 diphenylmethane	6·11	1·0
0·074	3·48	6·0	0·86
			Mean: 0·9 ± 0·2
0·026	2·7 2-methylpent-2-ene	11·5	2·1
0·04	5·4	21	1·9
			Mean: 2·0 ± 0·1
0·038	2·3 2,3-dimethylbut-2-ene	15·5	3·4
0·14	3·2	20·4	3·2
			Mean: 3·3 ± 0·1

[a] k_{obs} is the pseudo-first order rate constant for decay of absorbance at 800 nm. When $[RH]_0 < 10[Radical]_0$, k_{obs} was calculated from the initial rate of decay.

more pronounced than that from any spin contamination.

In both molecules, the two HCN bond angles are different, with the hydrogen atom *anti* to the oxygen having a bond angle approximately 7° larger in formaldoxime. The energy profiles in Figure 4 represent approximately the minimum energy pathways for the inversion of both molecules. The UMP2/6–31G(d) and UMP4/6–31G(d) results show that the inversion barrier for the iminoxyl radical is about 10 kcal mol^{-1} versus about 62 kcal mol^{-1} for the oxime. An inversion barrier of 9.6 kcal mol^{-1} has been calculated[22] from NMR data on **8**, a value of 12·5 kcal mol^{-1} calculated from ESR data on the iminoxyl from *p*-chlorobenzaldoxime,[23] while a theoretical value of 8·92 kcal mol^{-1} (INDO method) was estimated from a vinylic iminoxyl as a model for that iminoxyl.[23]

Mode of iminoxyl decomposition

Although the details of the decomposition pathways of the new radicals are not entirely clear, Scheme 2 can account for the traces of nitriles and the absence of the parent ketone among the decomposition products. The earliest part of the decomposition may be approximated by considering the initial steps:

$$\mathbf{1} \underset{k_{-1}}{\overset{k_1}{\rightleftharpoons}} \mathbf{1}' \xrightarrow{k_2} \text{dimer}$$

Table 4. Optimized results for H_2CNO

	ROHF 6–31g(d)	UHF 6–31g(d)	UMP2 6–31g(d)	UMP4 6–31g(d)	UMP2 6–31++G(2df,p)
Energy (a.u.	−168·2302	−168·2392	−168·6711	−168·7115	−168·7946
E (PUHF)[a]		−168·2558	−168·2491	−168·2510	−168·2725
E(PUMP2)[a]			−168·6844	−168·6843	−168·8076
NO	1·2746	1·2444	1·2184	1·2316	1·2059
CN	1·2531	1·2786	1·2442	1·2537	1·2379
H_1C	1·0770	1·0753	1·0872	1·0910	1·0860
H_2C	1·0717	1·0703	1·0803	1·0843	1·0785
Θ(CNO)	121·0	124·5	140·1	137·3	141·2
$\Theta(H_1CN)$	122·9	122·1	120·6	121·0	120·0
$\Theta(H_2CN)$	117·2	117·2	118·0	117·8	117·7
$\langle S^2 \rangle$	0·75	1·01	0·94	0·96	0·92

[a] UHF and UMP2 energies calculated with the quartet component projected out.

Table 5. Optimized results for H_2CNOH

	UHF 6–31g(d)	MP2 6–31g(d)	MP4 6–31g(d)	Experiment[a]
Energy (a.u.)	−168·8410	−169·3208	−169·3481	
NO	1·369	1·4091	1·4181	1·408
CN	1·249	1·2826	1·2888	1·276
H_1C	1·1.078	1·0881	1·0928	1·085
H_2C	1·073	1·0827	1·0874	1·086
HO	0·947	0·9732	0·9744	0·956
Θ(CNO)	112·0	110·0	109·9	110·5
Θ(H_1CN)	122·6	122·8	122·8	121·8
Θ(H_2CN)	117·3	116·4	116·4	115·5
Θ(HON)	104·5	102·0	101·9	102·7

[a] Data from Ref. 18.

$$d[\text{dimer}]/dt = -2d[\mathbf{1}]/dt = k_2[\mathbf{1}][\mathbf{1}'] = k_1k_2[\mathbf{1}]^2/(k_1+k_2[\mathbf{1}])$$

If k_1 is fast relative to the rate of trapping, then

$$d[\text{dimer}]/dt = K_{eq}k_2[\mathbf{1}]^2 = (k_{obs}/2)[\mathbf{1}]^2$$

The equilibrium constant $K_{eq} = k_1/k_{-1}$ can be estimated as

$$K_{eq} = [\mathbf{1}']/[\mathbf{1}] \approx A\, e^{(80\cdot9 - DH/\text{kcal})/RT}$$

where A is a statistical correction for the different numbers of β-hydrogens assumed to participate in the equilibrium and DH is the C–H bond strength of the reactive β-hydrogen.[24] The O–H bond strength in **8H** was assumed to be representative and has previously been measured calorimetrically as 80·9 kcal mol^{-1}.[25] For radicals **5** and **1** at 25 °C, we calculate $K_{eq} = 6\cdot9\times10^{-6}$ and $3\cdot1\times10^{-11}$, respectively. The *ratio* of these values, $2\cdot2\times10^5$, is in fact within an order of magnitude of the *ratio* of the observed second-order rate constants for the decay of **5** and **1** (Table 3: $0\cdot56/4\times10^3 = 4\times10^4$). Similarly, K_{eq} for the presumed intermediate radical **10** in Scheme 2 is calculated to be 10^3 times larger than for **1**, and we would expect iminoxyl **10** to be considerably less stable than **1** towards internal H abstraction and subsequent reactions.

At high concentrations, with $k_{-1} < k_2[\mathbf{1}]$, the rate of decay of iminoxyls that undergo internal H abstraction should be limited by the first-order rate of formation of the isomeric radicals. We were tempted to interpret the apparent overlap in the decay curves for **1** at the two highest concentrations (Figure 2) according to this condition, but our data, obtained by double integrations of the ESR signal over a period of days, were of limited accuracy. However, the decay of **1** dissolved in neat di-*tert*-butyl nitroxide (Figure 3) was

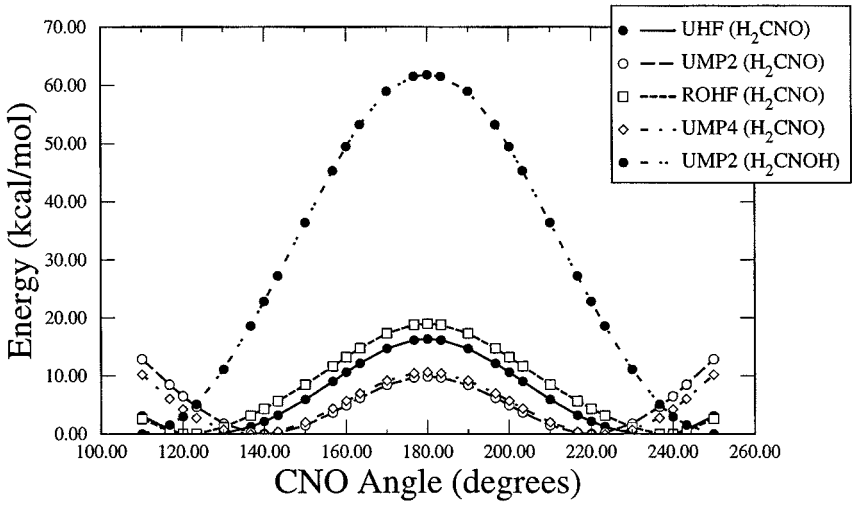

Figure 4. Relative energy profiles (kcal mol^{-1}) for the isomerization of formaldoxime, CH_2NOH, and the corresponding iminoxyl radical, CH_2NO, as a function of the CNO angle. At each angle, all other geometrical parameters were optimized. The 6–31g(d) basis was used for all cases

measured under conditions where the relative precision was greater and the reaction mixture remained homogeneous. A semilogarithmic plot of the relative concentration of **1** vs time gave an excellent fit ($r^2 = 0.994$) to first-order kinetics with $k_{obs} = 9.83 \times 10^{-6}\ s^{-1}$ ($t_{1/2} = 20$ h), corresponding to the prediction at the high-concentration limit. However, it should be noted that our kinetic methods determine the total iminoxyl concentration, which may include derivatized iminoxyls in Scheme 2.

The other significant inference that we may draw from Figure 2 is that a unimolecular scission of one bulky alkyl from the iminoxyl to give an alkyl cyanate:

$$R_1R_2C{=}NO^{\bullet} \rightarrow [R_1C{\equiv}NO + R_2^{\bullet}] \xrightarrow{fast} \text{other products}$$

is not a major decay path at room temperature, since the rate of decomposition by this pathway should, to a first approximation, be first order at all iminoxyl radical concentrations.

The energy differences between two model, straight-chain iminoxyls and their H-abstracted isomers were calculated byMO methods at the MP2/6–31g(d) level of theory with the geometries established at the UHF/6–31g level. The relative energies, shown under each structure below, further support preferential abstraction of the methylene proton. The energy differences beween the pairs of isomeric carbon- and oxygen-centered radicals are each about 3 kcal mol^{-1} larger than those we calculate from the bond strengths of related compounds.[24,25] However, attempts to locate the transition state for H-transfer in the system were unsuccessful (see Table below).

The degree and effects of the spin contamination for these molecules are similar to those for the H_2CNO radical. For all cases above, the expectation values of the spin angular momentum, $\langle S^2 \rangle$, were all in the range 0·9–1·0, which necessitated some analysis of the effects of the spin contamination. The relative energies were determined at the same UHF/6–31g geometries using the ROHF/6–31g(d) method and the PUMP2 energies determined from the UMP2/6–31g(d) results. For all values above, there was only a modest increase of 2–3 kcal mol^{-1} in the relative energies. A further test was made by re-optimizing the geometries to obtain the ROHF/6–31g(d)//ROHF/6–31g energies for CH_3CH_2CHNO and CH_2CH_2CHNOH. There was essentially no change in the relative energy when compared with the ROHF/6–31g(d)//UHF/6–31g results.

Influence of oxygen

From Scheme 2, one would predict that the presence of oxygen might slow the rate of disappearance of **1** by (a) regenerating the radical from the iminyl ($R_2C{=}N^{\bullet}$) or (b) converting carbon-centered radicals (**1′** and $R^{\bullet}$), which otherwise might combine with **1**, to peroxyl radicals, which can abstract hydrogen from **1H** and regenerate **1**. The oxygen might also increase in the rate of decay by trapping **1′**. Four experiments with 2 and 0·2 M **1** in acetonitrile under N_2 or O_2 at 23 °C were carried out with analysis of aliquots by HPLC. At the same starting concentration, the differences in rates of decay were comparable to the scatter in the data. At the higher concentration, the radical in each case decomposed faster, and under N_2 showed a reasonable fit to first-order kinetics to 70% loss of **1**, with $k_{obs} = 2{\cdot}3 \times 10^{-5}\ s^{-1}$. This rate constant is not that for internal H-abstraction (k_1) because it includes subsequent reactions that also destroy **1** (Scheme 2).

Iminoxyl derivatives of olefins

The rate constants measured for several compounds with activated hydrogens (Table 3; column 4 is the rate constant for H abstraction per molecule, if the stoichiometry of the reactions is the same as for cyclohexene) are interesting in that they are slower on a per-H basis for the more electron-rich tri- and tetrasubstituted ethylenes than for cyclohexene. Absolute rate constants for the *tert*-butoxyl radical, which are many orders of magnitude faster,[26] show the opposite pattern. Apparently the additional alkyl substitution increases steric hindrance of the approach of the iminoxyl so much that it offsets any advantage of increased electron density in the olefin.

CONCLUSIONS

Attempts to prepare kinetically more stable iminoxyl radicals by increasing the size of the surrounding alkyl groups has been frustrated by the appearance of new modes of decomposition, which result in complicated mixtures of products. In some cases, the calculated equilibrium constant between a radical and its more reactive, H-abstracted isomer appears to be a rough guide to relative persistence. The reaction of di-*tert*-butyl ketiminoxyl (**8**) with olefins is unusually selective and may be of synthetic utility.

	$CH_3CH_2CH_2CH{=}NO^{\bullet}$	$CH_3CH^{\bullet}CH_2CH{=}NOH$	$^{\bullet}CH_2CH_2CH_2CH{=}NOH$
E (au)	−286·16460	−286·13532	−286·13092
E_{rel} (kcal)	0	+12	+18

	$CH_3CH_2CH{=}NO^{\bullet}$	$^{\bullet}CH_2CH_2CH{=}NOH$
E (au)	−244·99859	−244·96432
E_{rel} (kcal)	0	+21

ACKNOWLEDGEMENTS

This work was carried out with support from the US Army Research Office (grant DAAG 29-78-C-001), the donors of the Petroleum Research Fund, administered by the American Chemical Society, an undergraduate fellowhip to M.N. from the Dean's office of MTU and a Dow Undergraduate Summer Fellowship to B.M.E. We also thank Mr Thomas Neils, Mr Brent Walchuk and Mr Kent R. Larson for experimental assistance, Mr David Lindsay at the National Research Council of Canada, Ottawa, for the LC–MS analyses, Mr Jerry Lutz for conventional mass spectra and Dr Ted M. McKinney for ESR simulation software. One of us (R.E.B.) thanks the National Science Foundation and in particular the NSF Supercomputer Center at Pittsburgh for a grant of computer resources (Grant CHE890022P).

REFERENCES

1. (a) J. R. Thomas, *J. Am. Chem. Soc.* **86**, 1446 (1964); (b) B. C. Gilbert, V. Malatesta and R. O. C. Norman, *J. Am. Chem. Soc.* **93**, 3290 (1971), and preceding papers in this series.
2. J. L. Brokenshire, J. R. Robers and K. U. Ingold, *J. Am. Chem. Soc.* **94**, 7040 (1972), and references cited therein.
3. P. L. Feldman, O. W. Griffith, H. Hong and D. J. Stuehr, *J. Med. Chem.* **36**, 491 (1993).
4. G. D. Mendenhall and K. U. Ingold, *J. Am. Chem. Soc.* **95**, 2963 (1973).
5. P. A. S. Smith, *Open-Chain Nitrogen Compounds*, Vol. II, pp. 56–60. Benjamin, New York (1966).
6. D. Lindsay, E. C. Horswill, D. W. Davidson and K. U. Ingold, *Can. J. Chem.* **52**, 3554 (1974).
7. B. M. Eisenhauer, M. Wang, H. Labaziewicz, M. Ngo and G. D. Mendenhall, *J. Org. Chem.* **62**, 2050 (1997).
8. M. Frisch, G. W. Trucks, M. Head-Gordon, P. M. W. Gill, M. W. Wong, J B. Foresman, B. G. Johnson, H. B. Schlegel, M. A. Robb, E. S. Replogle, R. Gomperts, J. L. Andres, K. Raghavachari, J. S. Binkley, C. Gonzalez, R. L. Martin, D. J. Fox, D. J. Defrres, J. Baker, J. J. P. Stewart and J. A. Pople, *Gaussian 92*. Gaussian, Pittsburgh, PA (1992).
9. H. B. Schlegel, *J. Comput. Chem.* **3**, 214 (1982).
10. (a) P. C. Hariharan and J. A. Pople, *Theor. Chim. Acta* **28**, 213 (1973); (b) M. J. Frisch, J. A. Pople and J. S. Binkley, *J. Chem. Phys.* **80**, 3265 (1984) and references cited therein.
11. G. D. Mendenhall and K. U. Ingold, *J. Am. Chem. Soc.* **95**, 627 (1973).
12. G. D. Mendenhall, D. Griller, W. Van Hoff and K. U. Ingold, *J. Am. Chem. Soc.* **96**, 6068 (1974).
13. V. W. Bowry and K. U. Ingold, *J. Am. Chem. Soc.* **114**, 4992 (1992).
14. T. M. McKinney, *ESR Simulation Program*.
15. W. M. Fox and M. C. R. Symons, *J. Chem. Soc. A* 1503 (1966).
16. A. Alberti, G. Barbaro, A. Battaglia, M. Guerra, F. Bernardi, A. Dondoni and G. F. Pedulli, *J. Org. Chem.* **46**, 742 (1981); an iminoxyl C–N–O bond angle around 140° has been calculated with an AM1 program: S. F. Nelsen, University of Wisconsin, personal communication.
17. W. J. Hehre, L. Radom, P. v. R. Schleyer and J. Pople, *Ab Initio Molecular Orbital Theory*, 1st ed., Chap. 6. Wiley, New York (1986).
18. I. N. Levine, *J. Chem. Phys.* (2326 (1963).
19. L. L. Merritt, Jr, and E. Lanterman, *Acta Crystallogr.* **5**, 811 (1952).
20. B. Jerslev, *Nature (London)* **166**, 742 (1950).
21. (a) C. Sosa, J. Andzehm, C. Lee, J. Blake, B. L. Chinard and T. W. Butler, *Int. J. Quantum Chem.* **49**, 511 (1994); (b) A. H. Otto, *THEOCHEM* **81**, 489 (1991); (c) R. Glazer and A. Streitweiser, *J. Am. Chem. Soc.* **111**, 7340 (1989) and references cited therein.
22. K. U. Ingold and S. Brownstein, *J. Am. Chem. Soc.* **97**, 1817 (1975).
23. M. Lucarini, G. F. Pedulli and A. Alberti, *J. Org. Chem.* **59**, 1980 (1994).
24. (a) Benzyl C–H bond strength in cumyl *tert*-butyl ketoxime assumed to be 84·7 kcal mol^{-1} as estimated for ethylbenzene: M. J. Rossi, D. F. McMillen and D. M. Golden, *J. Phys. Chem.* **88**, 5031 (1984); (b) Other C–H bond strengths assumed equivalent to the C–H in propane (CH_2, 95·1±1) and neopentane (100±2): D. F. McMillen and D. M. Golden, *Annu. rev. Phys. Chem.* **33**, 493 (1982); the CH BDE in **10** (Scheme 2 was equated to that of diethyl ether (91·7±0·4): O. Kondo and S. W. Benson, *Int. J. Chem. Kinet.* **16**, 949 (1984).
25. L. R. Mahoney, G. D. Mendenhall and K. U. Ingold, *J. Am. Chem. Soc.* **95**, 8610 (1973).
26. J. A. Howard and J. C. Scaiano, in *Radical Reaction Rates in Liquids*, Landolt-Bornstein, Vol. 13d, edited by H. Fischer, pp. 15*ff*. Springer, Berlin (1984).

